PHILOSOPHICAL MAGAZINE, 21 September 2003
VOL. 83, NO. 27, 3133–3157

Taylor & Francis
Taylor & Francis Group

Dislocation climb and low-temperature plasticity of an Al–Pd–Mn quasicrystal

F. MOMPIOU†, L. BRESSON‡, P. CORDIER§ and D. CAILLARD†||

†Centre d'Elaboration de Matériaux et d'Etudes Structurales, CNRS, BP 4347, 31055 Toulouse Cedex, France
‡Laboratoire d'Etudes des Matériaux, CNRS–ONERA, BP 72, 92322 Châtillon Cedex, France
§Laboratoire de Structures et Propriétés de l'Etat Solide, Unité Mixte de Recherche associée au CNRS 8008, Université des Sciences et Techniques de Lille, 59655 Villeneuve d'Ascq Cedex, France

[*Received 14 January 2003 and accepted in revised form 29 May 2003*]

ABSTRACT

Dislocations and phason faults have been studied by transmission electron microscopy in an Al–Pd–Mn sample deformed at 300°C under a high pressure. All dislocation movements have occurred by climb, in contrast with the usual interpretations of dislocation motion in quasicrystals. Several modes of dissociation and decomposition of dislocations have been observed, allowing for estimations of phason fault and antiphase-boundary energies. Work softening is tentatively explained in terms of a varying chemical stress.

§ 1. INTRODUCTION

Icosahedral quasicrystals exhibit a plastic behaviour at high temperatures which is controlled by the multiplication and the motion of dislocations (Wollgarten *et al.* 1993). Dislocations in Al–Pd–Mn single grains deformed at high temperatures (650–800°C) have been analysed by transmission electron microscopy (TEM) by Wollgarten *et al.* (1995) and Rosenfeld *et al.* (1995). They are perfect dislocations, with Burgers vectors equal to translation vectors of the six-dimensional lattice. However, since they form an isotropic three-dimensional network, their plane of motion could not be determined. *In-situ* experiments have also been carried out by Messerschmidt *et al.* (1999), in the same temperature range. The planes of motion could be identified but not the corresponding Burgers vectors.

In spite of the lack of independent experimental determinations of Burgers vectors and planes of motion, a glide movement has been postulated, in the plane containing the dislocation line direction and the Burgers vector component $\mathbf{b}_{//}$ in the physical space. Several models of glide have been subsequently proposed by Feuerbacher *et al.* (1997) and Takeuchi *et al.* (2002), and the corresponding dislocation motion has been simulated (Schaaf *et al.* 2000).

|| Email: caillard@cemes.fr.

Philosophical Magazine ISSN 1478–6435 print/ISSN 1478–6443 online
http://www.tandf.co.uk/journals
DOI: 10.1080/1478643031000155110

More recent studies, however, showed climb dislocation movements controlled by the diffusion of atomic species over large distances, without any evidence of pure glide (Caillard 2000, Caillard *et al.* 1999, 2000, 2002a,b). This analysis was possible because dislocations trailed stacking faults that could be used to determine the planes of motion. These stacking faults, also called 'phason faults', are the consequence of the non-periodicity of the quasicrystal lattice. They can be observed only after low-temperature deformation because they otherwise disappear by 'phason dispersion', or 'retiling', controlled by atomic diffusion (Caillard *et al.* 2003, Takeuchi 2003). In these experiments, the Burgers vector $\mathbf{b}_{//}$ was all along twofold directions of the physical space, and the climb planes were either twofold (perpendicular to $\mathbf{b}_{//}$) or fivefold (not containing $\mathbf{b}_{//}$). However, since the observations were made in as-grown alloys, that is under ill-defined temperature and stress conditions, the conclusions could not be safely extended to other situations.

We thus propose to describe in this article new experiments on Al–Pd–Mn single grains deformed at a low temperature, in order to avoid phason fault dispersion, and tentatively to increase the probability of dislocation motion by pure glide.

The experimental procedure is described first. Then, the results of TEM are analysed and the controlling mechanism is discussed.

§ 2. Experimental details

Single grains of icosahedral Al–Pd–Mn of nominal composition 70.1 ± 0.7 at.% Al–20.4 ± 0.2 at.% Pd–9.5 ± 0.1 at.% Mn were grown along a fivefold direction [1/0, 0/1, 0/0]† by the Czochralski method. A cylindrical sample (diameter, 3 mm; height, 3 mm) has been deformed in compression under a high pressure, in a multianvil apparatus, at the Laboratoire Magmas et Volcans in Clermont-Ferrand. The specimen is compressed in a high-pressure cell designed to generate high differential (compressive) stresses (Cordier and Rubie 2001). The pressure is first raised at room temperature to about 7 GPa in 7 h. The temperature is subsequently increased to 700 K and maintained for 30 min, while pressure is increased to 7.5 GPa to provide additional compression. The sample is then quenched to room temperature and the pressure is decreased slowly during 22 h to prevent damaging the anvils. After a total deformation of 7%, the sample remains cylindrical, with a higher surface roughness.

Slices have been cut in and 20° away from the $(1/0, 0/1, 0/0)$ fivefold plane perpendicular to the compression axis (see the stereographic projections in figures 1 (*a*) and (*b*)). They are called the first and second orientations in the following. The samples were then thinned by conventional ion milling under cooling. Other samples milled with a precision ion-polishing system did not contain any phason fault. In fact, this technique can introduce very high local heating (Viguier and Mortensen 2001), which can induce substantial phason fault retiling.

The samples have been observed in a JEOL 2010 HC electron microscope operating at 200 kV, in two-beam conditions, using different diffraction vectors parallel to twofold and fivefold directions. In the twofold direction, we have used the $[\tau]$ related vectors [20, 32] and [52, 84], denoted $\mathbf{g}_{2i(1)}$ and $\mathbf{g}_{2i(2)}$, where [N, M] is related to the modulus of the corresponding diffraction vector of the six-dimensional lattice according to $G^2 = N + M\tau$, $[\tau]$ is the matrix that inflates the parallel component by a

† In the notation of Cahn *et al.* (1989).

factor of τ (the golden mean) and deflates the perpendicular component by $1-\tau$, and N and M are given by Cahn *et al.* (1989). In the fivefold direction we have used the usual strong reflection [18, 29], denoted $\mathbf{g}_{5i}$ and the superstructure reflection [7, 11], according to the fact that the icosahedral structure can be seen as a six-dimensional superstructure of a primitive hypercubic lattice (Boudard *et al.* 1992). All these diffraction vectors must be used in order to proceed to the complete defect analysis.

§ 3. Rules of contrast

We have collected below a set of rules that are used to analyse dislocations. Some arise from the theoretical considerations of Wollgarten *et al.* (1991). Others are empirical but validated by large-angle convergent-beam electron diffraction experiments (Caillard *et al.* 2002a,b).

For perfect dislocations of the six-dimensional lattice, the rules of contrast are as follows:

(i) $\mathbf{G}\cdot\mathbf{B}=0$: no contrast for $\mathbf{g}_{//}\cdot(\mathbf{b}_{//}\times\mathbf{u})=0$, where $\mathbf{u}$ is parallel to the dislocation line direction, and strong residual contrast for large values of $\mathbf{g}_{//}\cdot(\mathbf{b}_{//}\times\mathbf{u})$;
(ii) $\mathbf{G}\cdot\mathbf{B}=1$: single contrast (see for example dislocation $2'$ in figure 8 (*a*) later);
(iii) $\mathbf{G}\cdot\mathbf{B}=2$: double contrast (see for example dislocation 2 in figure 8 (*a*) later).

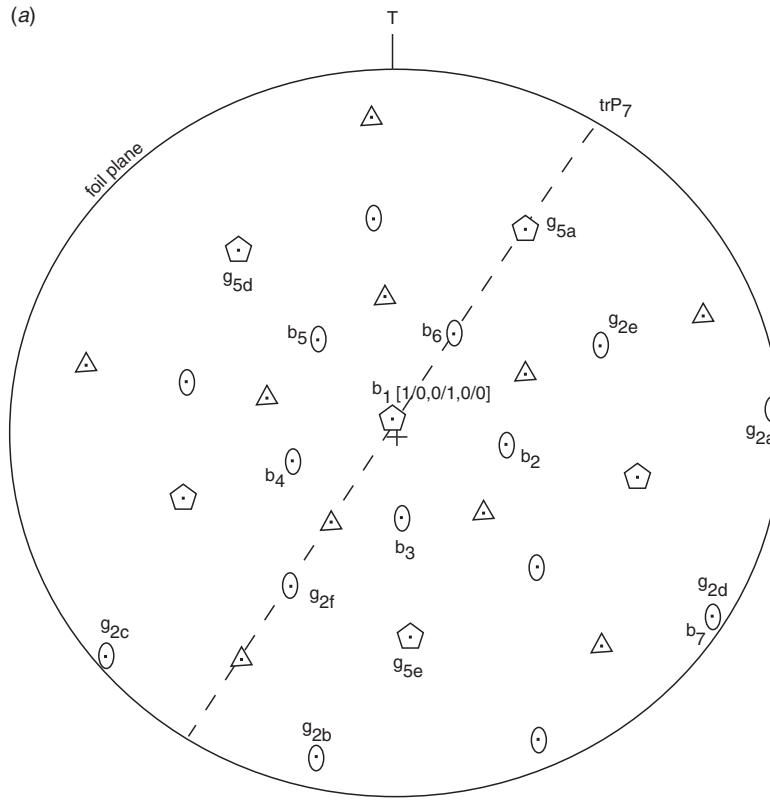

Figure 1. Stereographic projections of the two observed sample orientations: (*a*) perpendicular to the compression axis; (*b*) at 20° from the first axis. T and T′ are the tilt axes for TEM observations.

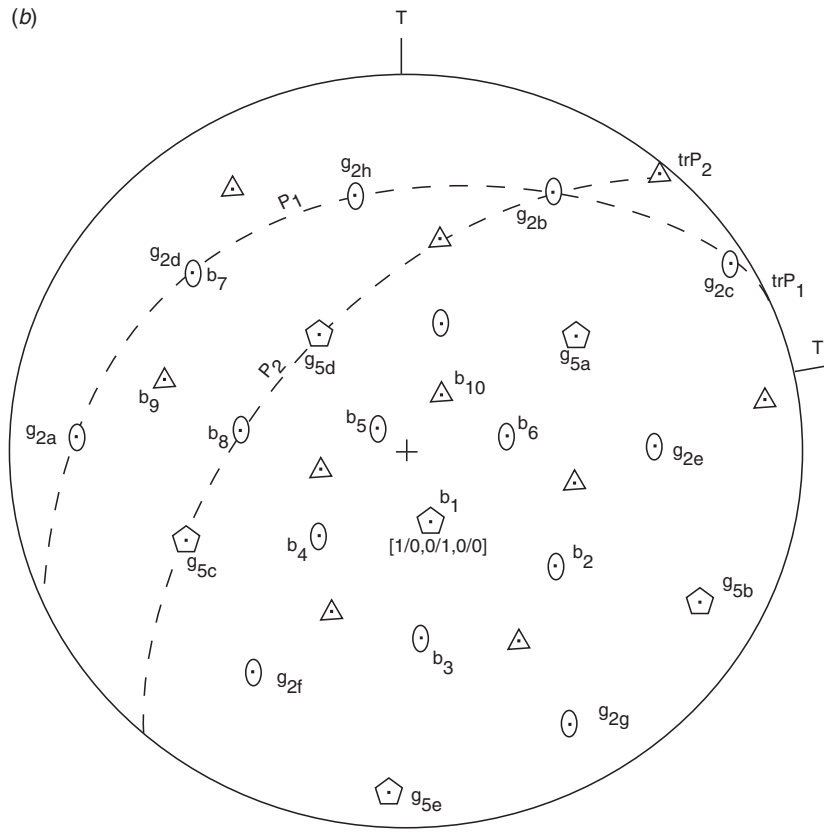

Figure 1. Continued.

Six independent equations $\mathbf{G}\cdot\mathbf{B}=$ integer are necessary to determine $\mathbf{B}$, one of these at least being $\mathbf{G}\cdot\mathbf{B}\neq\mathbf{0}$.

For non-retiled dislocations with $|\mathbf{b}_\perp|=0$, the scalar product in physical space is no longer integer, but the rules are the same as above as long as $\mathbf{g}_\perp\cdot\mathbf{b}_\perp\ll 1$, where $\mathbf{b}_\perp$ is the missing perpendicular component. Dislocations are out of contrast, or in residual contrast, for $\mathbf{g}_{//}\cdot\mathbf{b}_{//}=0$. Note that the phason faults trailed by dislocations are clearly out of contrast only in this case (see below)†. This observation can be used to identify ambiguous situations where $\mathbf{g}_{//}\cdot\mathbf{b}_{//}=0$, with strong residual contrast.

Differences between contrasts of retiled and non-retiled dislocations are important only where $\mathbf{g}_\perp\cdot\mathbf{b}_\perp$ is large. For instance, the weak extinction, observed on retiled dislocations where $\mathbf{g}_{//}\cdot\mathbf{b}_{//}=-\mathbf{g}_\perp\cdot\mathbf{b}_\perp$, cannot be obtained for non-retiled dislocations. The contrast is, however, very faint in this case, because $\mathbf{g}_{//}\cdot\mathbf{b}_{//}$ is substantially smaller than unity. This is called 'pseudoweak extinction'. It is observed where the dislocation line direction $\mathbf{u}$ is almost parallel to the diffraction vector, that is where

† For the same reason, dislocations in the condition $\mathbf{g}_{//}\cdot\mathbf{b}_{//}=0$ (e.g. dislocation 10 in figures 7(*g*) and (*h*)), moving in the wake of others for which $\mathbf{g}_{//}\cdot\mathbf{b}_{//}\neq 0$, do not alter their fringe contrast.

there is no additional 'residual-type' contrast ($\mathbf{g}_{//} \cdot (\mathbf{b}_{//} \times \mathbf{u}) = 0$). In this case, dislocations just appear as the limits of the phason fringe contrasts, as Shockley partials bounding a stacking fault, in crystals, under the condition $\mathbf{g} \cdot \mathbf{b}_p = \pm\frac{1}{3}$ (Howie and Whelan 1962). An example of a pseudoweak extinction is shown later in figure 4 (*m*) (dislocation 8). More generally, dislocations almost parallel to the diffraction-vector direction have the same very faint contrast when $\mathbf{g}_{//} \cdot \mathbf{b}_{//}$ is substantially smaller than unity (e.g. dislocation 9 in figure 5 (*i*)). In practice, non-retiled dislocations are analysed as if they were retiled, in the six-dimensional lattice, but their perpendicular components are set to zero. It must be verified subsequently that the scalar products $\mathbf{g}_{//} \cdot \mathbf{b}_{//}$ are either close to integer values, or consistent with a pseudoweak extinction. However, this procedure does not allow one to discriminate between partial retiling and no retiling at all.

The contrast of any stacking fault can be described by the scalar product $\mathbf{G} \cdot \mathbf{R}$ where $\mathbf{R}$ is the displacement vector in the six-dimensional space. The contrast is the same for $\mathbf{G} \cdot \mathbf{R}$ values differing by integer values. In the case of phason faults, the displacement vector is $\mathbf{r}_{//}$ in the physical space. Note that the corresponding contrast can be described by the quantity $\mathbf{g}_\perp \cdot \mathbf{r}_\perp$ as well, because both quantities differ by an integer value ($\mathbf{g}_{//} \cdot \mathbf{r}_{//} = -\mathbf{g}_\perp \cdot \mathbf{r}_\perp + \mathbf{G} \cdot \mathbf{R}$). The fault is considered in the first case to be created by a displacement in the physical space, whereas it is considered in the second case as a chemical fault created by a displacement in the perpendicular space. The contrast is described by rules deduced from those established for crystals and summarized by Gevers (1972). They have been adapted to the six-dimensional space.

(i) The fringe contrast is symmetrical in bright field and is reversed with the sign of $\mathbf{g}_{//}$.
(ii) The fringe contrast is asymmetrical in dark field and is reversed with the sign of $\mathbf{g}_{//}$.
(iii) When the phase shift is close to π ($\mathbf{g}_{//} \cdot \mathbf{r}_{//} \approx \frac{1}{2} + \text{integer}$), the fringe contrast is symmetrical, reversed when switching from bright to dark field, and independent of the sign of $\mathbf{g}_{//}$.
(iv) Planar faults are out of contrast for $\mathbf{g}_{//} \cdot \mathbf{r}_{//}$ integer. For phason faults, this condition reduces to $\mathbf{g}_{//} \cdot \mathbf{r}_{//} = 0$.

§ 4. Observations and interpretations

In the following, since there is no retiling around dislocations ($\mathbf{b}_\perp = \mathbf{0}$), all Burgers vectors have components only in the physical space.

4.1. *General observations*

Samples cut in the plane near (1/0, 0/1, 0/0) (first orientation) exhibit an homogeneous density of long and curved dislocations (figure 2 (*a*)). This shows that dislocations have moved in the plane perpendicular to the compression axis. No fringe contrast can be seen in their wake, except when the foil thickness is irregular, namely when the foil surface is locally slightly different from the average surface. This indicates that stacking faults (presumably phason faults) are present but parallel to the average foil plane. Indeed, since wave intensities oscillate with the distance to the surface, only inclined faults exhibit fringe patterns.

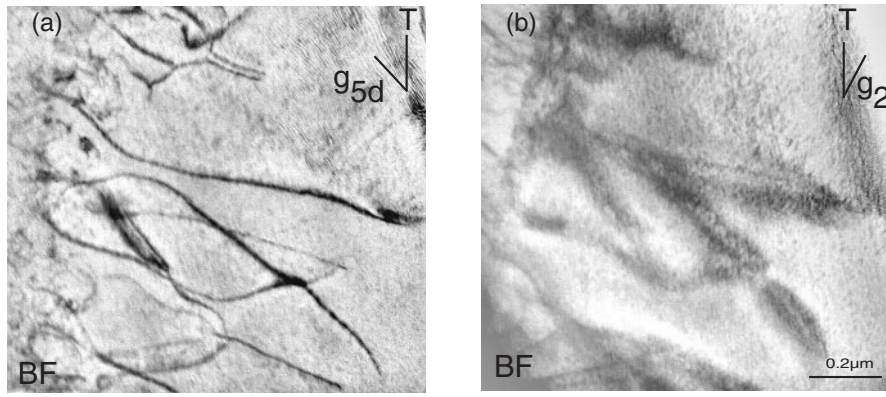

Figure 2. Dislocations with fivefold Burgers vectors parallel to the compression axis, in planes perpendicular to the compression axis (orientation 1). Dislocations are visible in (*a*) and in strong residual contrast in (*b*).

A contrast analysis has been made using the diffraction vectors plotted in the stereographic projection in figure 1 (*a*). Several dislocation families have been identified.

A large number of dislocations are out of contrast or in residual contrast with the twofold diffraction vectors parallel to the foil plane ($\mathbf{g}_{2a}$, $\mathbf{g}_{2b}$, $\mathbf{g}_{2c}$ and $\mathbf{g}_{2d}$). Their Burgers vector $\mathbf{b}_{//1}$ is accordingly parallel to the fivefold direction of the compression axis [1/0, 0/1, 0/0]. Figure 2 (*a*) shows these dislocations in contrast with the condition $\mathbf{g}_{2c} \cdot \mathbf{b}_{//1} = 0.94$. The same dislocations are in strong residual contrast in figure 2 (*b*), because the quantity $\mathbf{g} \cdot (\mathbf{b}_{//} \times \mathbf{u})$ is maximum for $\mathbf{g} \perp \mathbf{u}$. Other dislocations moving in the same plane have Burgers vectors parallel to several twofold directions out of the plane of motion.

The other dislocations have moved in different twofold planes. They are similar to those described in a previous article (Caillard *et al.* 2000). In particular, their Burgers vectors are always in the twofold directions perpendicular to their plane of motion. A large number of these dislocations have Burgers vectors $\mathbf{b}_{//2}, \ldots, \mathbf{b}_{//6}$ at 31.71° from the compression axis. Others have been observed in planes parallel to the compression axis, for example those with Burgers vector $\mathbf{b}_{//7}$ seen edge on in figure 3. The bright lines parallel to trP_7 correspond to the phason faults trailed in these planes. Note that some of the fivefold dislocations described above can also be seen in the upper right of the figure (in residual contrast).

These general observations show that all dislocations have moved either by pure climb or by a composite movement involving a large component of climb, hereafter called mixed climb. Conversely, no pure glide has been observed. The different climb systems are now studied in detail.

4.2. *Dislocations in the fivefold plane perpendicular to the compression axis*

The following observations have been performed in samples cut 20° from the compression plane (second orientation, see figure 1 (*b*)).

The faults in the (1/0, 0/1, 0/0) fivefold plane are now clearly visible. Dislocation motion in this plane appears highly planar. Two leading dislocations, distant from a few tens of nanometres, are followed by dislocations with different Burgers vectors which react with each other.

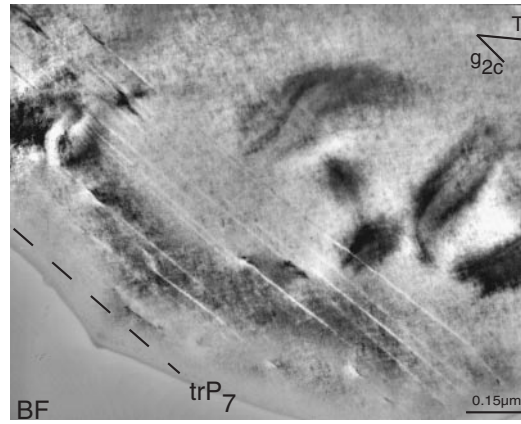

Figure 3. Phason faults and dislocations in planes parallel to the compression axis, seen edge on (orientation 1). Note the residual contrast of the same fivefold dislocations as in figure 2, in the top right corner.

4.2.1. *Leading dislocation pairs*

Figure 4 shows two leading dislocations, denoted 1 and 1′, trailing a fault, under various diffraction conditions. The direction of the fault trace (trP_1), and the variation in its apparent width as a function of the tilt angle, corresponds exactly to the $(1/0, 0/1, 0/0)$ fivefold compression plane, denoted P_1, already identified in the preceding section.

The fault left by the two leading dislocations has the usual characteristics of stacking faults: symmetrical fringe contrast in bright field, changing in $\pm\mathbf{g}$ conditions (v-shaped markers in figures 4(*c*) and (*d*)), and asymmetrical fringe contrast in dark field (v-shaped markers in figure 4(*b*)). The two leading dislocations are out of contrast for $\mathbf{g}_{2d(1)}$ (figure 4(*k*)) and $\mathbf{g}_{2d(2)}$ (figure 4(*l*)). They also exhibit a broad residual contrast for $\mathbf{g}_{2a(1)}$ (figure 4(*f*)), $\mathbf{g}_{2a(2)}$ (figure 4(*g*)), $\mathbf{g}_{2b(1)}$ and $\mathbf{g}_{2b(2)}$ (figure 4(*h*)), $\mathbf{g}_{2c(1)}$ (figure 4(*i*)) and $\mathbf{g}_{2c(2)}$ (figure 4(*j*)). In addition, the fault is clearly out of contrast in the same conditions. This shows that the Burgers vectors are perpendicular to $\mathbf{g}_{2a}$, $\mathbf{g}_{2b}$, $\mathbf{g}_{2c}$ and $\mathbf{g}_{2d}$, namely parallel to the direction $[1/0, 0/1, 0/0]$ denoted $\mathbf{b}_1$. These dislocations are the same as those already observed in samples with the first orientation. Additional information can be obtained from the double contrasts observed with $\mathbf{g}_{2e(2)}$ and $\mathbf{g}_{2g(2)}$, which are typical of $\mathbf{g}_{//} \cdot \mathbf{b}_{//} \approx 2$ (figures 4(*n*) and (*p*)). All results are summarized in table 1.

If the dislocations were perfect, their Burgers vector would be $\mathbf{B}_1 = [100000]$. Taking into account the absence of any retiling, which is obvious at this temperature, the Burgers vector is reduced to its physical component $\mathbf{b}_{//1} = [1/0, 0/1, 0/0]$, of length 0.456 nm.

According to the fact that [100000] is not a translation of the six-dimensional F structure, but only a translation of the six-dimensional primitive cubic sublattice, we conclude that the dislocation pairs are the projection in the physical space of a superdislocation with Burgers vector [200000], dissociated in two superpartials separated by an antiphase-boundary (APB) ribbon. The contrast of this fault is discussed below, and dislocation 8 is analysed in §4.2.3. Since the Burgers vector of the leading pair is $2\mathbf{b}_{1//}$, projection of a translation vector of the six-dimensional lattice ($2\mathbf{B}_1$), the fault left behind the pair is a phason fault.

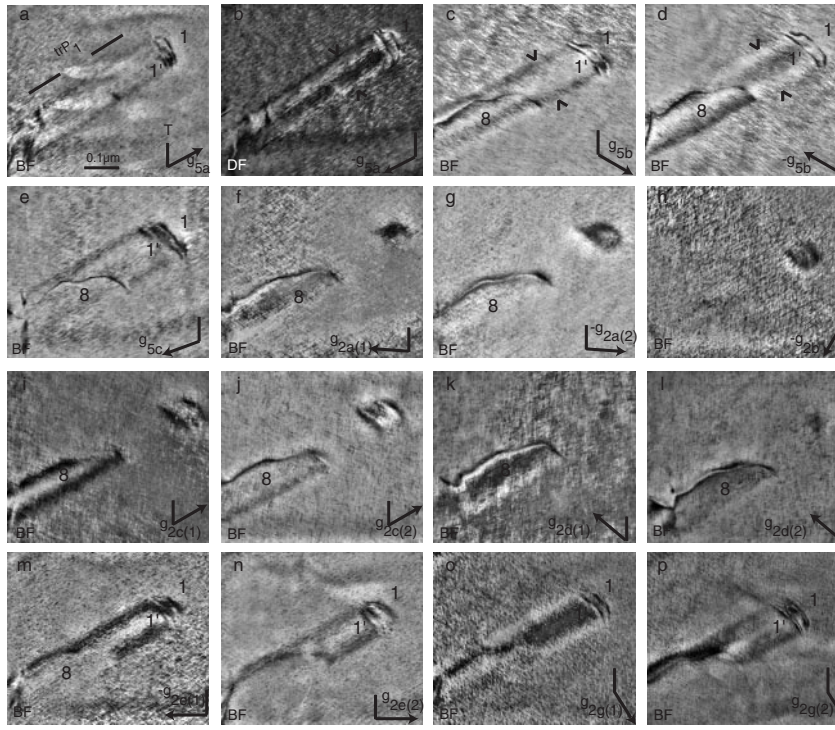

Figure 4. Dislocations moving in the fivefold plane perpendicular to the compression axis (orientation 2). The superdislocation dissociated into two superpartials 1 and 1′ is followed by another dislocation denoted 8. The fringe contrast of the phason fault trailed by the couple 1–1′ is indicated by v-shaped markers in (*b*) dark-field and (*c*) bright-field conditions.

Table 1. Contrast conditions for superpartial dislocations with Burgers vector $\mathbf{b}_{//1} = [1/0, 0/1, 0/0]$.

$\mathbf{g}$	$\mathbf{g}_{//}$	$\mathbf{g}_{//} \cdot \mathbf{b}_{//1}$	$\mathbf{G} \cdot \mathbf{B}_1$[a]	Figure 4[b,c]	Figure 5[b,c]
$\mathbf{g}_{5a}$	$0/0, 1/2, 2/3$	0.94	1	(*a*), (*b*)	
$\mathbf{g}_{5b}$	$\bar{1}/\bar{2}, 2/3, 0/0$	0.94	1	(*c*), (*d*)	(*a*)
$\mathbf{g}_{5b[7,11]}$	$\bar{1}/\bar{1}, 1/2, 0/0$	0.59	0.5		(*b*)
$\mathbf{g}_{5c}$	$2/3, 0/0, \bar{1}/\bar{2}$	0.94	1	(*e*)	
$\mathbf{g}_{2a(1)}$	$\bar{2}/\bar{3}, 1/2, 1/1$	0	0	(*f*) (E)	(*c*) (E)
$\mathbf{g}_{2a(2)}$	$\bar{3}/\bar{5}, 2/3, 1/2$	0	0	(*g*) (E)	(*d*) (E)
$\mathbf{g}_{2b(1)}$	$0/0, 0/0, \bar{2}/\bar{4}$	0	0	(*h*) (E)	(*e*) (E)
$\mathbf{g}_{2b(2)}$	$0/0, 0/0, \bar{4}/\bar{6}$	0	0		
$\mathbf{g}_{2c(1)}$	$1/2, \bar{1}/\bar{1}, \bar{2}/\bar{3}$	0	0	(*i*) (E)	(*f*) (E)
$\mathbf{g}_{2c(2)}$	$2/3, \bar{1}/\bar{2}, \bar{3}/\bar{5}$	0	0	(*j*) (E)	
$\mathbf{g}_{2d(1)}$	$\bar{2}/\bar{3}, 1/2, \bar{1}/\bar{1}$	0	0	(*k*) (E)	(*g*) (E)
$\mathbf{g}_{2d(2)}$	$\bar{3}/\bar{5}, 2/3, \bar{1}/\bar{2}$	0	0	(*l*) (E)	(*h*) (E)
$\mathbf{g}_{2e(1)}$	$\bar{1}/\bar{1}, 2/3, 1/2$	1.17	1	(*m*)	
$\mathbf{g}_{2e(2)}$	$\bar{1}/\bar{2}, 3/5, 2/3$	1.89	2	(*n*) (D)	
$\mathbf{g}_{2g(1)}$	$\bar{1}/\bar{1}, 2/3, \bar{1}/\bar{2}$	1.17	1	(*o*)	(*i*)
$\mathbf{g}_{2g(2)}$	$\bar{1}/\bar{2}, 3/5, \bar{2}/\bar{3}$	1.89	2	(*p*) (D)	(*j*) (D)

[a] $\mathbf{G} \cdot \mathbf{B}_1$ would be the phase shift if retiling was possible.
[b] E, extinction.
[c] D, double contrast.

4.2.2. *Complex fault analysis*

Figure 5 shows another similar pair of leading dislocations (1 and 1′). The fault between the two dislocations 1 and 1′ is the projection of the APB in the physical space. It is accordingly a complex fault with two components: an APB and a phason fault. When imaged with the superstructure diffraction vector $\mathbf{g}_{5b[7,11]} = [\bar{1}/\bar{1}, 1/2, 0/0]$, the APB yields a phase shift of π, and the phason fault yields a small additional phase shift $0.085 \times 2\pi$. The total phase shift is accordingly $0.585 \times 2\pi$, as mentioned in table 1. Since it is close to π, it yields the symmetrical dark field contrast observed in figure 5 (*b*) (v-shaped markers). The dark-field image with $\mathbf{g}_{5b[18,29]} = [\bar{1}/\bar{2}, 2/3, 0/0]$, shown for comparison (figure 5 (*a*)), yields the usual asymmetrical fringe contrast, in agreement with the phase shift $0.94 \times 2\pi$.

Figure 6 shows a cut of the six-dimension space, with the three possible superpartial displacement vectors (arrows) that project in the physical space along the [1/0, 0/1, 0/0] direction, and the corresponding phase shifts. The [100000] superpartial

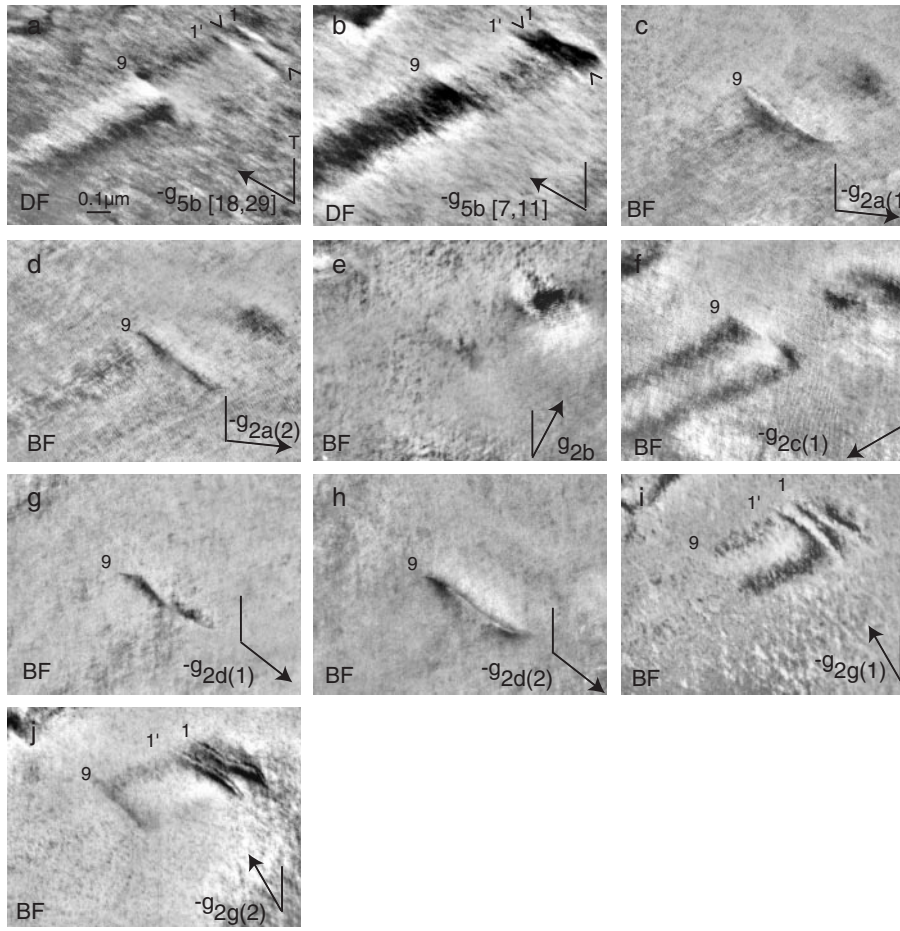

Figure 5. Dislocations moving in the fivefold plane perpendicular to the compression axis (orientation 2). The superdislocation 1–1′ is followed by a superpartial dislocation denoted 9. Note the contrast of the complex fault (APB + phason fault) in a dark field with the superstructure diffraction vector $\mathbf{g}_{5b[7,11]}$ in (*b*).

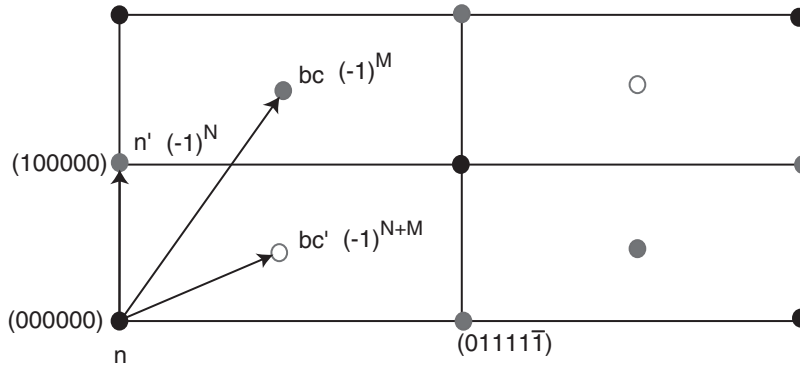

Figure 6. Cut of the six-dimensional space showing different possible superpartial Burgers vectors, projecting in the physical space along a fivefold direction, and corresponding phase shifts.

is the only one for which the phase shift $(-1)^N = \exp(-2i\pi \mathbf{G}\cdot\mathbf{R})$ is consistent with the observations, that is equal to -1 for $N=7$ and $M=11$, and equal to 1 for $N=18$ and $M=29$ (Cornier-Quiquandon *et al.* 1991).

The π contrast is erased by the second superpartial $1'$ of the pair (figure 5 (*b*)). It is replaced by the normal asymmetrical fringe contrast corresponding to a two times larger phase shift equal to $1.17 \times 2\pi$. The π contrast is, however, restored by a third dislocation denoted 9 which is accordingly another superpartial. It is also described in the following section.

4.2.3. *Dislocations in the wake of leading pairs*

Dislocation 8, which follows the leading superdislocation 1–$1'$ in the same fivefold plane in figure 4, is analysed in table 2. It is out of contrast for $\mathbf{g}_{5a}$ (figures 4 (*a*) and (*b*)) and $\mathbf{g}_{2b(1)}$ and $\mathbf{g}_{2b(2)}$ (figure 4 (*h*)). Its Burgers vector is accordingly along the twofold direction denoted $\mathbf{b}_8$ (figure 1 (*b*)). On the basis of its double contrast in $\mathbf{g}_{2a(2)}$ (figure 4 (*g*)) and $\mathbf{g}_{2d(2)}$ (figure 4 (*l*)), its Burgers vector is found to be $\mathbf{b}_{//8} = [2/2,\ 0/0,\ 0/0]$, of length 0.296 nm.

The superpartial dislocation 9 of figure 5 has another Burgers vector. On the basis of its extinction for $\mathbf{g}_{2b}$ (figure 5 (*e*)) and double contrast for $\mathbf{g}_{2d(2)}$ (figure 5 (*h*)), its Burgers vector is found to be $\mathbf{b}_{//9} = [\bar{1}/0,\ 2/\bar{1},\ 0/0]$ (see table 3) (its sign will be discussed in § 5.1.3). It is along the threefold direction denoted $\mathbf{b}_9$ in figure 1 (*b*). Its length is 0.257 nm, equal to the shortest interatomic distance in the structure model (Boudard *et al.* 1992). Since it is only 11° from the $(1/0, 0/1, 0/0)$ plane of motion, dislocation motion involves a large component of shear.

4.2.4. *Decomposition of fivefold dislocations*

Figure 7 shows dislocations moving in the same fivefold plane as above. An isolated dislocation, denoted $1'$, is followed by a group of three reacting dislocations, denoted 1, 3, and 10. All dislocations and phason faults are out of contrast with $\mathbf{g}_{2a(1)}$ and $\mathbf{g}_{2a(2)}$ (figure 7 (*d*)). Dislocations 1 and $1'$ are also invisible for $\mathbf{g}_{2c(1)}$ (figure 7 (*e*) and $\mathbf{g}_{2c(2)}$ (figure 7 (*f*)) and they exhibit a double contrast for $\mathbf{g}_{2f(2)}$ (figure 7 (*h*)). They are accordingly the same fivefold superpartials as above, with the Burgers vector $\mathbf{b}_{//1} = [1/0, 0/1, 0/0]$ of length 0.456 nm (table 4). Dislocation 3 is out of contrast for $\mathbf{g}_{5a}$ (figure 7(*a*)) and for $\mathbf{g}_{2a(1)}$ and $\mathbf{g}_{2a(2)}$ (figure 7 (*d*)), and it has a double contrast

Table 2. Contrast conditions for dislocation with Burgers vector $\mathbf{b}_{//8} = [\bar{2}/2, 0/0, 0/0]$.

$\mathbf{g}$	$\mathbf{g}_{//}$	$\mathbf{g}_{//} \cdot \mathbf{b}_{//8}$	$\mathbf{G} \cdot \mathbf{B}_8$[a]	Figure 4[b]
$\mathbf{g}_{5a}$	$0/0, 1/2, 2/3$	0	0	(*a*), (*b*) (E)
$\mathbf{g}_{5b}$	$\bar{1}/\bar{2}, 2/3, 0/0$	−0.72	−1	(*c*), (*d*)
$\mathbf{g}_{5c}$	$2/3, 0/0, \bar{1}/\bar{2}$	0.72	1	(*e*)
$\mathbf{g}_{2a(1)}$	$\bar{2}/\bar{3}, 1/2, 1/1$	−1.17	−1	(*f*)
$\mathbf{g}_{2a(2)}$	$\bar{3}/\bar{5}, 2/3, 1/2$	−1.89	−2	(*g*) (D)
$\mathbf{g}_{2b(1)}$	$0/0, 0/0, \bar{2}/\bar{4}$	0	0	(*h*) (E)
$\mathbf{g}_{2b(2)}$	$0/0, 0/0, \bar{4}/\bar{6}$	0	0	
$\mathbf{g}_{2c(1)}$	$1/2, \bar{1}/\bar{1}, \bar{2}/\bar{3}$	0.72	1	(*i*)
$\mathbf{g}_{2c(2)}$	$2/3, \bar{1}/\bar{2}, \bar{3}/\bar{5}$	1.17	1	(*j*)
$\mathbf{g}_{2d(1)}$	$\bar{2}/\bar{3}, 1/2, \bar{1}/\bar{1}$	1.17	1	(*k*)
$\mathbf{g}_{2d(2)}$	$\bar{3}/\bar{5}, 2/3, \bar{1}/\bar{2}$	1.89	2	(*l*) (D)
$\mathbf{g}_{2e(1)}$	$\bar{1}/\bar{1}, 2/3, 1/2$	−0.44	0	(*m*) (PWE)
$\mathbf{g}_{2e(2)}$	$\bar{1}/\bar{2}, 3/5, 2/3$	−0.72	−1	(*n*)
$\mathbf{g}_{2g(1)}$	$\bar{1}/\bar{1}, 2/3, \bar{1}/\bar{2}$	−0.44	0	(*o*) (PWE)
$\mathbf{g}_{2g(2)}$	$\bar{1}/\bar{2}, 3/5, \bar{2}/\bar{3}$	−0.72	−1	(*p*)

[a] $\mathbf{G} \cdot \mathbf{B}_8$ would be the phase shift if retiling was possible.
[b] E, extinction; PWE, pseudoweak extinction; D, double contrast.

Table 3. Contrast conditions for dislocation with Burgers vector $\mathbf{b}_{//9} = [\bar{1}/0, 2/\bar{1}, 0/0]$.

$\mathbf{g}$	$\mathbf{g}_{//} \cdot \mathbf{b}_{//9}$	$\mathbf{G} \cdot \mathbf{B}_9$[a]	Figure 5[b]
$\mathbf{g}_{5b}$	0.95	1	(*a*)
$\mathbf{g}_{5b[7,11]}$	0.59	0.5	(*b*)
$\mathbf{g}_{2a(1)}$	1.17	1	(*c*)
$\mathbf{g}_{2a(2)}$	1.89	2	(*d*)
$\mathbf{g}_{2b(1)}$	0	0	(*e*) (E)
$\mathbf{g}_{2b(2)}$	0	0	
$\mathbf{g}_{2c(1)}$	−0.72	−1	(*f*)
$\mathbf{g}_{2d(1)}$	1.17	1	(*g*)
$\mathbf{g}_{2d(2)}$	1.89	2	(*h*) (D)
$\mathbf{g}_{2g(1)}$	0.72	1	(*i*)
$\mathbf{g}_{2g(2)}$	1.17	1	(*j*)

[a] $\mathbf{G} \cdot \mathbf{B}_9$ would be the phase shift if retiling was possible.
[b] E, extinction; D, double contrast.

for $\mathbf{g}_{2f(2)}$ (figure 7(*h*)). It is accordingly a twofold dislocation with Burgers vector $\mathbf{b}_{//3} = [2/\bar{1}, 1/0, 1/\bar{1}]$ of length 0.296 nm. Note the pseudoweak extinction for $\mathbf{g}_{2c(1)}$ (figure 7(*e*)). Dislocation 10 is out of contrast for $\mathbf{g}_{2a(1)}$ and $\mathbf{g}_{2a(2)}$, (figure 7(*d*)) and for $\mathbf{g}_{2f(1)}$ (figure 7(*g*)) and $\mathbf{g}_{2f(2)}$ (figure 7(*h*)) note the continuity of the fringe contrast across the dislocation in strong residual contrast). Its Burgers vector is accordingly parallel to the threefold direction denoted $\mathbf{b}_{10}$. Taking into account the single contrast in $\mathbf{g}_{2c(2)}$ (figure 7(*f*)) and the pseudoweak extinctions for example in $\mathbf{g}_{5c}$ (figure 7(*c*)), the Burgers vector is likely to be $\mathbf{b}_{//10} = [\bar{1}/1, \bar{1}/1, \bar{1}/1]$ of length 0.257 nm. As dislocations 1 and 1′, dislocation 10 is the projection in the physical space of a superpartial dislocation of the six-dimensional F hypercubic lattice.

Dislocations 1, 3 and 10 react according to

$$[1/0, 0/1, 0/0] \rightarrow [2/\bar{1}, 1/0, 1/\bar{1}] + [\bar{1}/1, \bar{1}/1, \bar{1}/1].$$

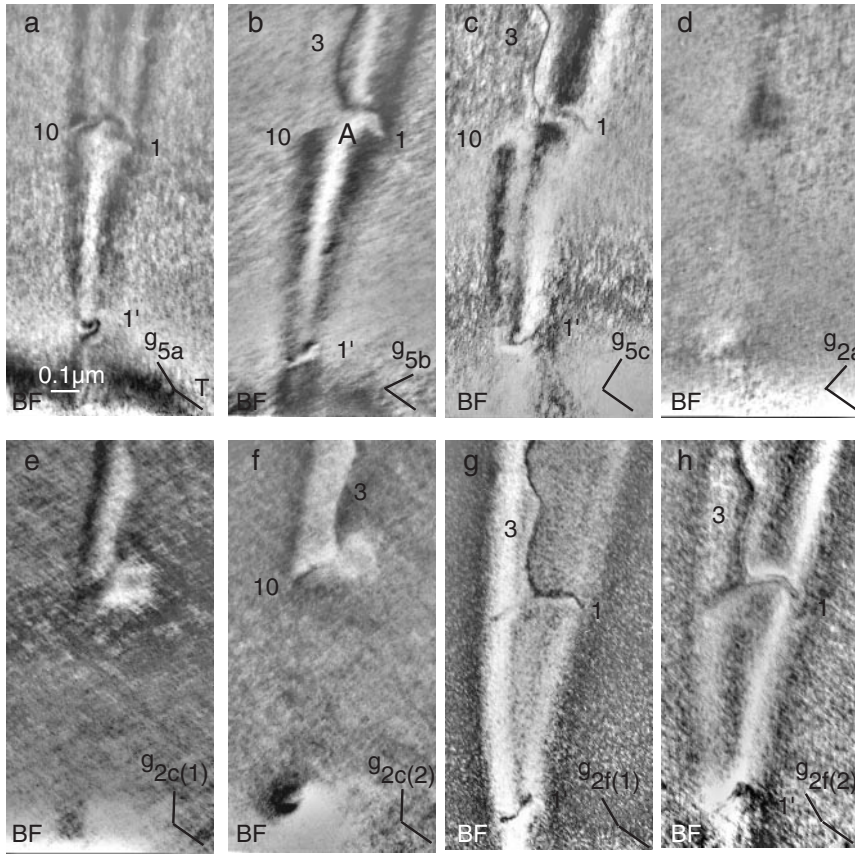

Figure 7. Three reacting dislocations 1, 3 and 10 in a fivefold plane perpendicular to the compression axis. The superpartial 1 decomposes into the normal dislocation 3 and the superpartial 10.

Table 4. Contrast conditions for dislocations with Burgers vectors $\mathbf{b}_{//1} = [1/0, 0/1, 0/0]$, $\mathbf{b}_{//3} = [2/\bar{1}, 1/0, 1/\bar{1}]$, and $\mathbf{b}_{//10} = [\bar{1}/1, \bar{1}/1, \bar{1}/1]$.

g	Figure 7	$\mathbf{g}_{//} \cdot \mathbf{b}_{//1}$	$\mathbf{G} \cdot \mathbf{B}_1$[a]	Contrast $1^{b,c}$	$\mathbf{g}_{//} \cdot \mathbf{b}_{//3}$	$\mathbf{G} \cdot \mathbf{B}_3$[a]	Contrast $3^{b,c}$	$\mathbf{g}_{//} \cdot \mathbf{b}_{//10}$	$\mathbf{G} \cdot \mathbf{B}_{10}$[a]	Contrast $10^{b,d}$
$\mathbf{g}_{5a}$	(*a*)	0.95	1	V	0	0	E	0.95	1	V
$\mathbf{g}_{5b}$	(*b*)	0.95	1	V	0.72	1	V	0.22	0	PWE
$\mathbf{g}_{5c}$	(*c*)	0.95	1	V	0.72	1	V	0.22	0	PWE
$\mathbf{g}_{2a(1)}$	(*d*)	0	0	E	0	0	E	0	0	E
$\mathbf{g}_{2a(2)}$		0	0		0	0		0	0	
$\mathbf{g}_{2c(1)}$	(*e*)	0	0	E	0.45	0	PWE	−0.45	0	PWE
$\mathbf{g}_{2c(2)}$	(*f*)	0	0	E	0.72	1	V	−0.72	−1	V
$\mathbf{g}_{2f(1)}$	(*g*)	1.17	1	V	1.17	1	V	0	0	E
$\mathbf{g}_{2f(2)}$	(*h*)	1.89	2	D	1.89	2	D	0	0	E

[a] Phase shifts would be $\mathbf{G} \cdot \mathbf{B}_i$ if retiling was possible.
[b] V, visible; E, extinction.
[c] D, double contrast.
[d] PWE, pseudoweak extinction.

4.3. *Dislocations in the twofold planes with normal at 31.71° from the compression axis*

Figure 8 shows two pairs of dislocations trailing phason faults. The trace direction, denoted trP_2, and the apparent width of the fault as a function of the tilt angle correspond to the plane perpendicular to the direction $\mathbf{b}_2$ (see figure 1 (*b*)). The leading dislocation of a pair is denoted 2, and the second dislocation is denoted 2′. Since both dislocations are out of contrast for $\mathbf{g}_{5c}$ and $\mathbf{g}_{2b(2)}$ (see figures 8 (*b*) and (*d*), their Burgers vectors are parallel to the twofold direction $\mathbf{b}_2$. This corresponds to a pure climb process. The leading dislocation 2 has a double contrast in $\mathbf{g}_{5b}$ (figure 8 (*a*)), whereas the trailing dislocation 2′ has a simple contrast under the same conditions. The same remark holds for $\mathbf{g}_{2d(2)}$ (figure 8 (*e*)) and $\mathbf{g}_{2g(1)}$ (figure 8 (*f*)). One can see a triple contrast on the leading dislocation versus a double contrast on the trailing dislocation, for $\mathbf{g}_{2g(2)}$ (figure 8 (*g*)). All results, summarized in table 5, are consistent with the Burgers vector $\mathbf{b}_{//2} = [0/0, 2/0, 0/0]$, of length 0.480 nm, for the leading dislocation, and $\mathbf{b}_{//2'} = [0/0, \bar{2}/2, 0/0]$, of length 0.296 nm, for the trailing dislocation. The Burgers vector length of the total dissociated dislocation is

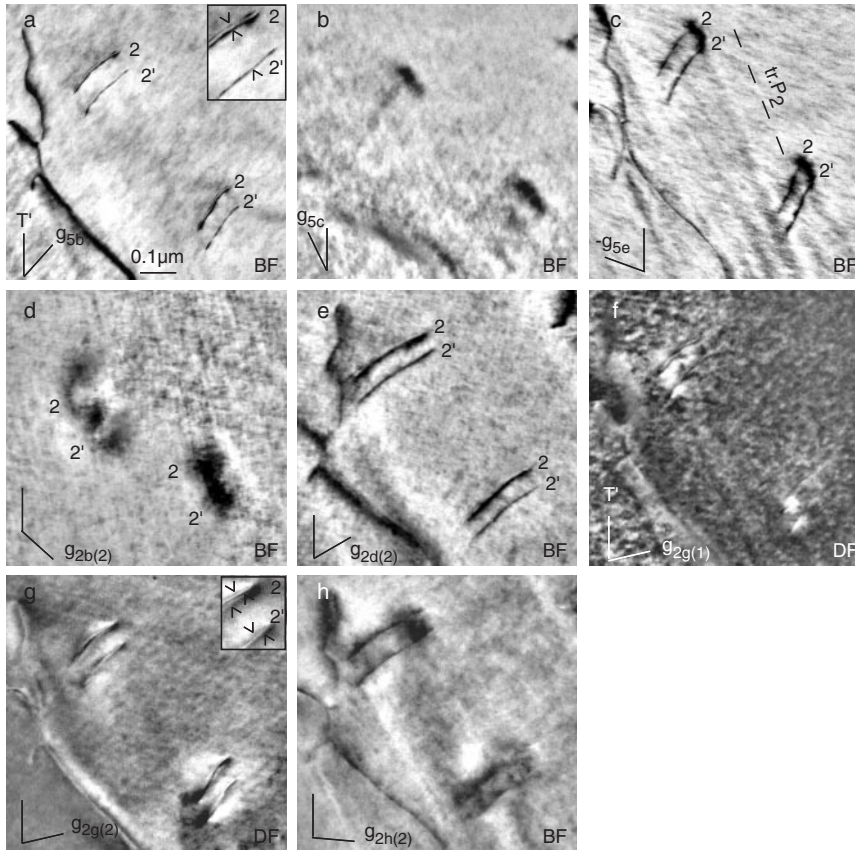

Figure 8. Dislocation pairs in twofold planes with normal at 32° from the compression axis. Note the double contrast of the leading dislocations in (*a*), and the triple contrast of the leading dislocations and the double contrast of the trailing dislocations in (*g*). The phason fault is clearly seen in (*c*).

Table 5. Contrast conditions for dislocations with Burgers vectors $\mathbf{b}_{//2} = [0/0, 2/0, 0/0]$ and $\mathbf{b}_{//2'} = [0/0, \bar{2}/2, 0/0]$.

$\mathbf{g}$	Figure 8	$\mathbf{g}_{//} \cdot \mathbf{b}_{//2}$	$\mathbf{G} \cdot \mathbf{B}_2$	Contrast $2^{b,c}$	$\mathbf{g}_{//} \cdot \mathbf{b}_{//2'}$	$\mathbf{G} \cdot \mathbf{B}_{2'}$	Contrast $2'^{b}$
$\mathbf{g}_{5b}$	(*a*)	1.89	2	D	1.17	1	V
$\mathbf{g}_{5c}$	(*b*)	0	0	E	0	0	E
$\mathbf{g}_{5e}$	(*c*)	1.17	1	V	0.72	1	V
$\mathbf{g}_{2b(2)}$	(*d*)	0	0	E	0	0	E
$\mathbf{g}_{2d(2)}$	(*e*)	1.89	2	D	1.17	1	V
$\mathbf{g}_{2g(1)}$	(*f*)	1.89	2	D	1.17	1	V
$\mathbf{g}_{2g(2)}$	(*g*)	3.07	3	T	1.89	2	D
$\mathbf{g}_{2h(2)}$	(*h*)	−1.17	−1	V	−0.72	−1	V

[a] Phase shifts would be $\mathbf{G} \cdot \mathbf{B}_i$ if retiling was possible.
[b] D, double contrast; E, extinction; V, visible.
[c] T, triple contrast.

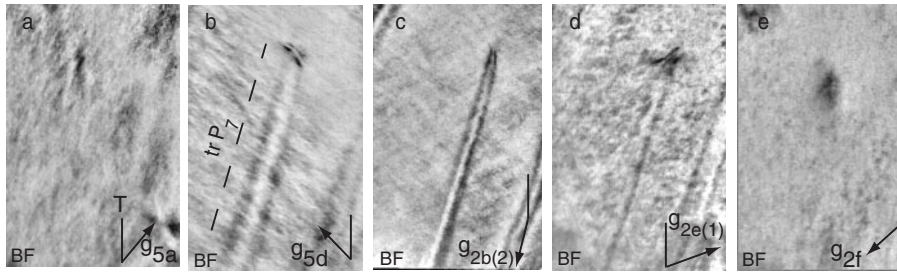

Figure 9. Dislocation 7 in a twofold plane parallel to the compression axis (orientation 1).

accordingly 0.776 nm. It is interesting to note that this length is τ times larger than that measured in a preceding study (Caillard *et al.* 2000). The dissociation width is about 70 nm.

4.4. *Dislocations in the twofold planes parallel to the compression axis*

The dislocations and phason faults seen edge on in figure 3 are analysed in figure 9. The trace (trP_7) and apparent width of the phason fault correspond to the twofold plane $(1/1, 0/\bar{1}, 1/0)$ perpendicular to the direction $\mathbf{b}_7$, and parallel to the compression axis.

Both phason faults and dislocations are out of contrast for $\mathbf{g}_{5a}$ (figure 9 (*a*)) and $\mathbf{g}_{2f(1)}$ and $\mathbf{g}_{2f(2)}$ (figure 9 (*e*)). This yields a Burgers vectors in the direction $\mathbf{b}_7$ perpendicular to the fault plane. On the basis of the double contrast† in $\mathbf{g}_{5d}$ (figure 9 (*b*)), the Burgers vector is determined to be $\mathbf{b}_{//7} = [0/1, \bar{1}/0, \bar{1}/1]$, of length 0.480 nm (table 6).

4.5. *'Vacancy or interstitial' character of phason faults*

The fringe contrast can be used to determine the character of phason faults. In fcc crystals, the intrinsic or extrinsic character of stacking faults can be determined

† The double contrast may be a decomposition into respectively τ times and τ^2 times smaller dislocations, as proposed by Caillard *et al.* (2000). The total Burgers vector would be the same.

Table 6. Contrast conditions for dislocations with Burgers vectors $\mathbf{b}_{//7} = [0/1, \bar{1}/0, \bar{1}/1]$.

$\mathbf{g}$	Figure 9	$\mathbf{g}_{//} \cdot \mathbf{b}_{//7}$	$\mathbf{G} \cdot \mathbf{B}_7$[a]	Contrast 7[b]	$\sin(2\pi \mathbf{g}_{//} \cdot \mathbf{b}_{//7})$[c]	Outer fringe
$\mathbf{g}_{5a}$	(*a*)	0	0	E		
$\mathbf{g}_{5d}$	(*b*)	1.89	2	D	−0.64	Dark
$\mathbf{g}_{2b(2)}$	(*c*)	−1.17	−1	V	−0.88	Dark
$\mathbf{g}_{2e(1)}$	(*d*)	−1.17	−1	V	−0.88	Dark
$\mathbf{g}_{2f(1)}$	(*e*)	0	0	E		
$\mathbf{g}_{2f(2)}$		0	0			

[a] Phase shifts would be $\mathbf{G} \cdot \mathbf{B}_7$ if retiling was possible.
[b] E, extinction; D, double contrast; V, visible.
[c] The values of $\sin(2\pi \mathbf{g}_{//} \cdot \mathbf{b}_{//7})$ and the character of the outer fringe are consistent with an interstitial-type phason fault.

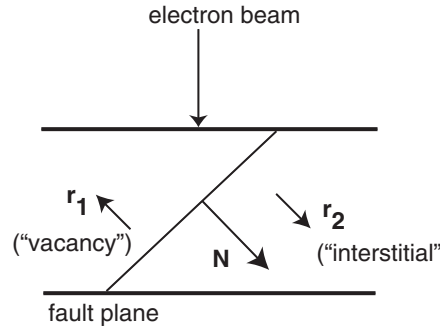

Figure 10. Rules given by Gevers (1972) for the determination of the vacancy or interstitial character of phason faults.

from their fringe contrast. The phase shift is $\alpha = 2\pi\, \mathbf{g}\cdot\mathbf{r}$. Following the rules given by Gevers (1972), for $\alpha \neq \pi(2\pi)$, namely, when the contrast is symmetrical in a bright field, the outer fringe is bright when $\sin\alpha > 0$, and dark when $\sin\alpha < 0$. Thus, knowing the diffraction vector with its sign, and the displacement vector $\mathbf{r}$ in length and direction, we can determine the sign of $\mathbf{r}_{//}$ by inspecting the nature of the outer fringe. The same rules are valid for phason faults in quasicrystals, with $\alpha = 2\pi \mathbf{g}_{//}\cdot\mathbf{r}_{//}$ (Caillard *et al*. 2003).

The displacement vector $\mathbf{r}_{//}$ is chosen to be equal to the Burgers vector of the corresponding dislocation. It has a component perpendicular to the phason plane in all studied cases. In order to avoid any confusion with fcc crystals where the same stacking fault can be obtained by shear and by precipitation of vacancies or interstitials, we use by analogy the denomination 'vacancy character' for phason faults obtained by removing matter, and 'interstitial character' for those obtained by adding matter.

The normal to the fault plane is oriented as indicated by Gevers (figure 10). The displacement vector is normal to the fault plane for all leading dislocations. When it is oriented as the normal to the fault plane, $\mathbf{N}$ (direction $\mathbf{r}_2$), the fault has an 'interstitial' character. It has a 'vacancy' character in the alternative case.

Returning to the phason fault trailed by dislocation pairs in the fivefold plane perpendicular to the compression axis (§ 4.2.1, figure 4), we obtain $\mathbf{r}_{//} = -\mathbf{N} = [2/0, 0/2, 0/0]$, which shows that the fault has a 'vacancy' character. Climb has accordingly occured by absorption of 'vacancies' or by emission of 'interstitials'. The same result

is obtained for dislocations climbing in twofold planes nearly perpendicular to the compression axis (§4.3, and figure 8). Conversely, the phason fault in the twofold plane parallel to the compression axis (§4.4, and figure 9) has a displacement vector $\mathbf{r}_{//} = \mathbf{N} = [0/1, \bar{1}/0, \bar{1}/1]$, namely it has an 'interstitial' character (see table 6). Climb in that case has occurred by emission of 'vacancies'.

§5. Discussion

These results unambiguously show that dislocation climb is a very active deformation mechanism, in agreement with our previous investigations (Caillard *et al.* 1999, 2000, 2002a,b). Even at half the melting temperature, there is no indication of dislocation motion by pure glide. All models which attempted to account for the mechanical properties of Al–Pd–Mn above 300°C, as well as those of other icosahedral quasicrystals, should accordingly be deeply revised (for example Feuerbacher *et al.* (1999)).

The dislocation dissociations and decompositions are first analysed quantitatively. Then, the different forces acting on the observed climb systems are estimated and discussed.

5.1. *Dissociations and decompositions*

Since split dislocations have components in the physical space that remain connected by phason faults, there is no clear difference between 'dissociation' and 'decomposition'. We use the first terminology when the two components remain parallel and close to each other, and the second in the alternative case. The discussion below is different from that of Wang *et al.* (1998) because the latter workers considered only perfect dislocations, namely neither superpartials nor phason and complex faults.

5.1.1. *Dissociation of fivefold dislocations*

According to §4.2.2, superdislocations with fivefold Burgers vectors dissociate in the six-dimensional space as in classical intermetallic alloys, into two superpartials separated by an APB ribbon. However, after projection on to the physical space, the two superpartials are separated by a complex fault, which can be described as the superposition of the APB and the phason fault trailed by the first superpartial. If the two corresponding surface energies are additive, the complex fault energy is $\gamma_{\mathrm{APB}} + \gamma_1$, where γ_1 is assumed to be proportional to the missing component $b_{\perp 1}$ of the superpartial Burgers vector $b_{//1}$. The phason fault trailed by the superdislocation has the surface energy $2\gamma_1$ (figure 11 (*a*)). F_{i} is the elastic repulsion between the two superpartials. In addition, both superpartials were subjected to the same applied force $\tau_{\mathrm{c}} b_{//1}$, where τ_{c} is the proper climb stress, calculated in §5.2.1. The forces on both superpartials can accordingly be decomposed into a symmetrical part $\gamma_{\mathrm{APB}} - F_{\mathrm{i}}$, which tends to narrow or widen the dissociation distance d, and an asymmetrical part $\tau_{\mathrm{c}} b_{//1} - \gamma_1$, which is at the origin of the motion (figure 11 (*b*)).

Assuming that the dissociated superdislocations have their equilibrium configurations, the APB energy can be deduced from the average dissociation distance d by the classical formula, deduced from the equilibrium condition $\gamma_{\mathrm{APB}} = F_{\mathrm{i}}$:

$$\gamma_{\mathrm{APB}} = \frac{\mu b_{//1}^2}{2\pi(1-\nu)d},$$

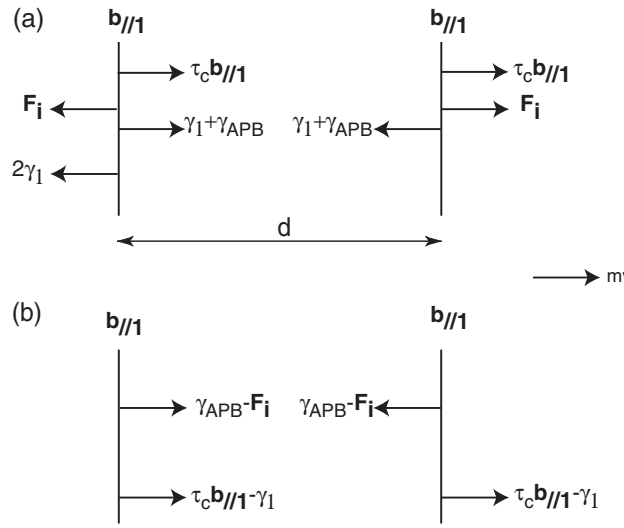

Figure 11. Forces acting on superpartial dislocations in fivefold planes. The symmetrical and asymmetrical components are shown in (*b*).

where $b_{//1}$ is the modulus of the Burgers vector of each superpartial in the physical space ($b_{//1} = 0.456$ nm), μ is the shear modulus ($\mu = 62.5$ GPa at 300°C, from Tanaka *et al.* (1996)), $1 - \nu \approx 0.75$, and $d \approx 40$ nm on average ($30\,\text{nm} < d < 60\,\text{nm}$, from ten measurements). This yields $\gamma_{\text{APB}} = 69\,\text{mJ}\,\text{m}^{-2}$. γ_{APB} ranges between the stacking-fault energies of Ni and Cu. It is more than twice the APB energy in {100} planes of Ni_3Al (Matterstock *et al.* 1999).

The surface energy $2\gamma_1$ of the phason fault trailed by the superdislocation cannot be estimated in this experiment.

5.1.2. *Dissociation of twofold dislocations*

Forces acting on the dislocations shown in figure 8 are described schematically in figure 12. The leading dislocation has the Burgers vector $b_{//2}$ of length 0.480 nm, and the trailing dislocation has the Burgers vector $b_{//2'} = b_{//2}/\tau$, of length 0.296 nm. If the phason fault trailed by the leading dislocation has the surface energy γ_2, the dislocation trailed by the total dislocation of Burgers vector $b_{//2}(1 + 1/\tau) = \tau b_{//2}$ has the surface energy γ_2/τ (this surface energy is assumed to be proportional to the missing component of the corresponding Burgers vector in the perpendicular space, which is divided by τ when the parallel component is multiplied by τ).

The equilibrium configuration under stress cannot be established unambiguously because the frictional forces opposing the motion of the two dislocations are *a priori* different. Under such conditions, the components of the forces devoted to dislocation motion are also different, and they cannot be identified with the asymmetrical part of the total forces, as above. We thus assume that the equilibrium dissociation distance is the same as in the absence of an external stress (figure 12). The asymmetrical part $\gamma_2/2\tau$ of the forces acting on dislocations corresponds to the back force γ_2/τ of the phason fault trailed by the dislocation pair shared between the leading and the trailing dislocations. The symmetrical part, which determines the dissociation

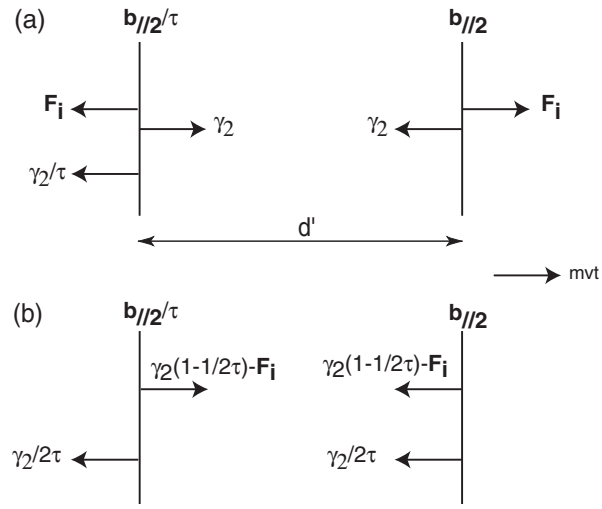

Figure 12. Forces acting on dislocation pairs in twofold planes. The symmetrical and asymmetrical components are shown in (*b*).

distance d', is then $\gamma_2(1-1/2\tau) - F_i$. Considering that the symmetrical part is zero at equilibrium yields

$$\gamma_2\left(1-\frac{1}{2\tau}\right) = \frac{\mu b_{//2}^2}{2\pi(1-\nu)\tau d'}.$$

The average dissociation width $d' \approx 70$ nm yields $\gamma_2 = 39\,\mathrm{mJ\,m^{-2}}$.

The phason fault trailed by the dislocation pair has the surface energy $\gamma_2/\tau = 24\,\mathrm{mJ\,m^{-2}}$. It is fairly low, of the same order of magnitude as the stacking-fault energy of Ag. It yields a back stress $\gamma_2/\tau b_{//2} = 31$ MPa.

Returning to the dissociation of fivefold dislocations, the phason fault energy γ_1 can be estimated assuming that it is only proportional to the length of the missing component $\mathbf{b}_\perp$ of the moving dislocation in the perpendicular space, that is that it is independent of the fault plane and direction of $\mathbf{b}_\perp$. This yields $2\gamma_1 = 24\,\mathrm{mJ\,m^{-2}} \times 0.912/0.480 = 46\,\mathrm{mJ\,m^{-2}}$, where 0.912 nm and 0.480 nm are the lengths of the missing perpendicular components of $2\mathbf{b}_{//1}$ and $\tau\mathbf{b}_{//2}$ respectively. It yields a back stress $2\gamma_1/2b_{//1} = 50$ MPa. The energy of the complex fault is accordingly of the order of $\gamma_{\mathrm{APB}} + \gamma_1 = 92\,\mathrm{mJ\,m^{-2}}$.

5.1.3. *Decomposition of fivefold superpartials*

The decomposition of a fivefold superpartial into a threefold superpartial and a twofold normal dislocation, described in §4.2.2.4, is energetically favourable because the Burgers vectors of the decomposition products are at 69° from each other in the physical space (figure 13). The elastic energy, proportional to $b_{//}^2$, is indeed decreased by the decomposition, in agreement with $b_{//3}^2 + b_{//10}^2 < b_{//1}^2$. The leading dislocation 10 trails a phason fault of energy proportional to $b_{\perp 10}$, which is to a large extent compensated by that trailed by dislocation 3 (figure 13). Since the fault in front of dislocation 10 is unknown, the role of faults in the decomposition process cannot, however, be estimated.

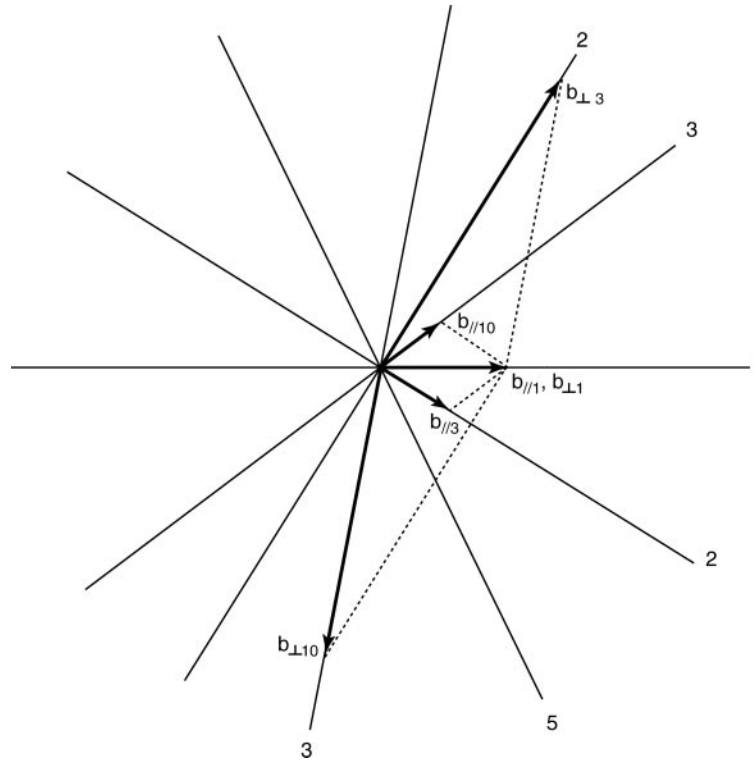

Figure 13. Reaction of decomposition of a fivefold superpartial ($\mathbf{b}_{//1}$) into a twofold dislocation ($\mathbf{b}_{//3}$) and a threefold superpartial ($\mathbf{b}_{//10}$) (see figure 7). The reaction between the missing perpendicular components, which represent the energy of the corresponding phason faults, is also shown.

Dislocations $\mathbf{b}_{//8}$ and $\mathbf{b}_{//9}$, observed in the wake of the leading superdislocations $2\mathbf{b}_{//1}$ (§4.2.3) have presumably a similar origin. The twofold dislocation $\mathbf{b}_{//8}$ seen in figure 4 can result from the decomposition of a superdislocation $2\mathbf{b}_{//1}/\tau$ according to $2\mathbf{b}_{//1}/\tau \rightarrow \mathbf{b}_{//8} + \mathbf{b}_{//2}$, or $[\bar{2}/2, 2/0, 0/0] \rightarrow [\bar{2}/2, 0/0, 0/0] + [0/0, 2/0, 0/0]$. This reaction may be possible although $\mathbf{b}_{//8}$ and $\mathbf{b}_{//2}$ are at right angles, in such a way that there is *a priori* no decrease in total elastic energy. Superdislocations $2\mathbf{b}_{//1}/\tau$ are expected to be present in the wake of the leading dislocations ($2\mathbf{b}_{//1}$) for energy reasons. Indeed, their respective perpendicular components are of opposite signs and tend to compensate each other, which leads to a decrease in the phason fault energy. The threefold dislocation seen in figure 5 has a Burgers vector $\mathbf{b}_{//9} = [\bar{1}/0, 2/\bar{1}, 0/0]$. The opposite vector can be rejected because it would yield for $\mathbf{g}_{2g(1)}$ and $\mathbf{g}_{2g(2)}$ a total phase shift which is incompatible with the faint fringe contrast observed behind the dislocation. Note that dislocation 9 accordingly removes a substantial fraction of the phason fault energy corresponding to the superdislocation $2\mathbf{b}_{//1}$. It may originate from the decomposition equation $\mathbf{b}_{//2} \rightarrow \mathbf{b}_{//1} + \mathbf{b}_{//9}$, although $\mathbf{b}_{//1}$ and $\mathbf{b}_{//9}$ are at 100° to each other, so that the decomposition is *a priori* not energetically favourable.

It is worth noting that only leading fivefold superpartials are coupled whereas the following superpartials are isolated and more likely to decompose. The origin of this behaviour is not understood at present.

5.2. *Mobilities of climbing dislocations*

5.2.1. *Stresses on climbing dislocations*

According to Hirth and Lothe (1992, p. 557), the hydrostatic pressure P does not induce dislocation climb in crystals. It, however, decreases the vacancy concentration from c_0, in the absence of pressure, to $c_0^{(P)} = c_0 \exp(-P\Omega/kT)$, where Ω is the atomic volume. We assume that these conclusions are also valid for quasicrystals. The external forces acting on climbing dislocations are then due to the compression stress only. We show below that the Schmid factor, defined for gliding dislocations, can also be used for pure and mixed climb.

Let α be the angle between the dislocation Burgers vector and the compression axis, and β the angle between the normal to the plane of motion and the compression axis. When one dislocation crosses the whole sample section, the work done by the external applied stress σ is $\sigma S_0 b \cos\alpha$, where S_0 is the sample section. It is equal to the work done by the force F per unit length acting on the climbing dislocation sweeping the area $S_0/\cos\beta$, which yields $F = \sigma b \cos\alpha \cos\beta$. The climb stress is thus $\tau_c = \sigma \cos\alpha \cos\beta$, and the Schmid factor is $\cos\alpha \cos\beta$, as in pure glide. It is interesting to note that the maximum Schmid factor is 1 when climb is allowed (case of pure climb with $\alpha = \beta = 0$) whereas it is only 0.5 in pure glide.

The driving forces $\tau_c b_{//}$ are decreased by the surface energies of the different faults, estimated in § 5.1 above.

5.2.2. *Velocities of climbing dislocations*

In crystals, the dislocation climb velocity can be written as

$$v = \frac{D}{b \cos^2 \psi} \frac{\Omega\tau}{kT} c_j,$$

where D is the self-diffusion energy of the slowest-diffusing species (vacancies in most cases), ψ is the angle between the Burgers vector and the climb plane normal ($\psi = 0$ for pure climb), Ω is the atomic volume and c_j is the jog concentration on the dislocation line. This equation is assumed to be valid for quasicrystals, although the different parameters involved do not yet have a clear meaning.

5.2.3. *Comparison between pure climb in twofold and fivefold planes*

Plastic deformation has been produced by a mixture of several pure climb systems: fivefold dislocations moving in the fivefold plane perpendicular to the compression axis, and twofold dislocations moving in the five twofold planes with the normal at 31° from the compression axis. The amounts of climb in the fivefold plane, on the one hand, and in all families of twofold planes, on the other hand, are equivalent. If the amount of strain per climb system is considered, the fivefold system is accordingly the most active. This can be related to its high Schmid factor (1, to be compared with $\cos^2 31.71^\circ = 0.72$ in the twofold planes). The higher resolved stress in the fivefold plane is counterbalanced by a higher phason fault energy (about 46 mJ m^{-2} versus 24 mJ m^{-2} in twofold planes). However, the corresponding frictional stresses (50 MPa and 31 MPa respectively) are probably negligible with respect to the compression stress. In conclusion, the most active system (the fivefold system) has the highest total driving stress. On the basis of this *a priori* logical behaviour, the mobilities of dislocations moving by pure climb in twofold and fivefold planes appear to be similar.

5.2.4. *Comparison between pure and mixed climb in fivefold planes*

Leading superdislocations have a Schmid factor of 1. Their velocity is that of one superpartial, namely

$$v = \frac{1}{b_{//1}} \frac{\Omega \sigma_c}{kT} c_j,$$

where the back forces due to the phason faults have been neglected. Dislocations in their wake are moving by mixed climb. The latter have a Schmid factor smaller than 1 because the angles α between their Burgers vectors and the compression axis are different from zero. Their expected velocity is

$$v' = \frac{1}{b_{//} \cos^2 \psi} \frac{\Omega \sigma_c \cos \alpha}{kT} c_j,$$

which, since $\alpha = \psi$, reduces to

$$v' = \frac{1}{b_{//} \cos \alpha} \frac{\Omega \sigma_c}{kT} c_j.$$

Since $v' > v$, their motion is controlled by the motion of the leading superpartial pair. The reason why mixed climb is never observed alone is not clear at present.

5.2.5. *Multiplication and climb in the twofold planes parallel to the compression axis, and work softening*

Since these climb systems have a zero Schmid factor, they are subjected to no mechanical stress. They must accordingly be activated by chemical forces that are always present at climbing dislocations. The whole mechanism is described in the following.

After some amount of climb, the average density of vacancies absorbed by the fivefold dislocations necessarily decreases. This induces a negative chemical stress, equal to

$$\tau^{(c)} = \frac{kT}{\Omega} \ln\left(\frac{c}{c_0^{(P)}}\right),$$

where c is the vacancy concentration at long distances from the dislocation cores and $c_0^{(P)}$ is the thermal equilibrium vacancy concentration under the hydrostatic pressure (Hirth and Lothe 1992). This stress opposes the external driving stress τ. This hardening effect can, however, be compensated by the nucleation and multiplication of dislocations acting as vacancy sources, for example those climbing in the twofold planes parallel to the compression axis (figure 14). These dislocations are indeed subjected to a positive chemical stress opposite to $\tau^{(c)}$. Their multiplication starts when $-\tau^{(c)}$ is sufficiently high, namely after some amount of strain.

The evolutions of the vacancy concentration c and associated chemical stresses are described schematically as a function of strain in figures 15 (*a*) and (*b*) respectively. In a first step, dislocations multiplying by climb in planes almost perpendicular to the compression axis (density ρ (figure 15 (*d*))) absorb available vacancies, which leads to an increase in the modulus of the negative chemical stress acting on them. In constant-strain-rate experiments, dislocation multiplication and increase in chemical stress at low strain (below ε_1) are responsible for the yield drop (figure 15 (*c*)). When the vacancy concentration c is low enough, dislocations start to move

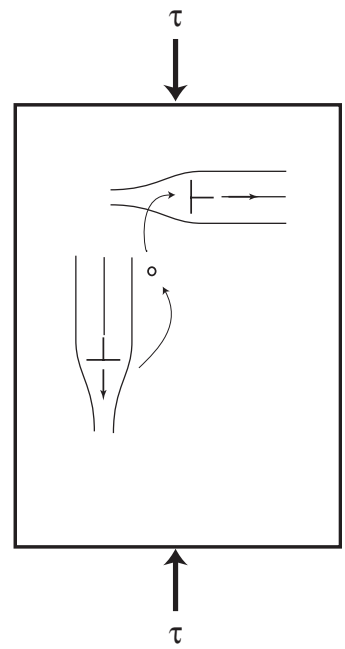

Figure 14. Vacancy flux between dislocations climbing in planes parallel and perpendicular to the compression axis.

and to multiply in the planes parallel to the compression axis (density ρ'), by emitting vacancies, under the positive chemical stress $-\tau^{(c)}$. This tends in turn to increase again the vacancy concentration and to decrease the flow stress. The latter phenomenon may be at the origin of the work softening observed at large strains (Feuerbacher *et al.* 1997). Indeed, since available explanations of work softening all rely on pure glide mechanisms (Mikulla *et al.* 1998, Brunner *et al.* 2000, Takeuchi *et al.* 2002, Messerschmidt and Bartsch 2003), new explanations must be proposed as climb appears to be the dominant process of plastic deformation.

§ 6. Conclusions

TEM observations of Al–Pd–Mn single grains deformed at 300°C under a high confining pressure have yielded the following results.

(1) Extensive motion of dislocations trailing phason faults has occurred during deformation.
(2) All dislocation movements involve a climb component. No indication of pure glide has been obtained. This confirms earlier studies and indicates that dislocation models proposed so far should be deeply revised.
(3) Dislocation pairs move by pure climb in twofold planes. The two components have Burgers vectors of length 0.480 nm and 0.296 nm, in the ratio of τ, the golden mean. The energy of the phason fault in between, corresponding to the dislocation of length 0.480 nm, is 39 mJ m^{-2}. The back stress of phason faults trailed by moving dislocations is negligible with respect to the applied stress.

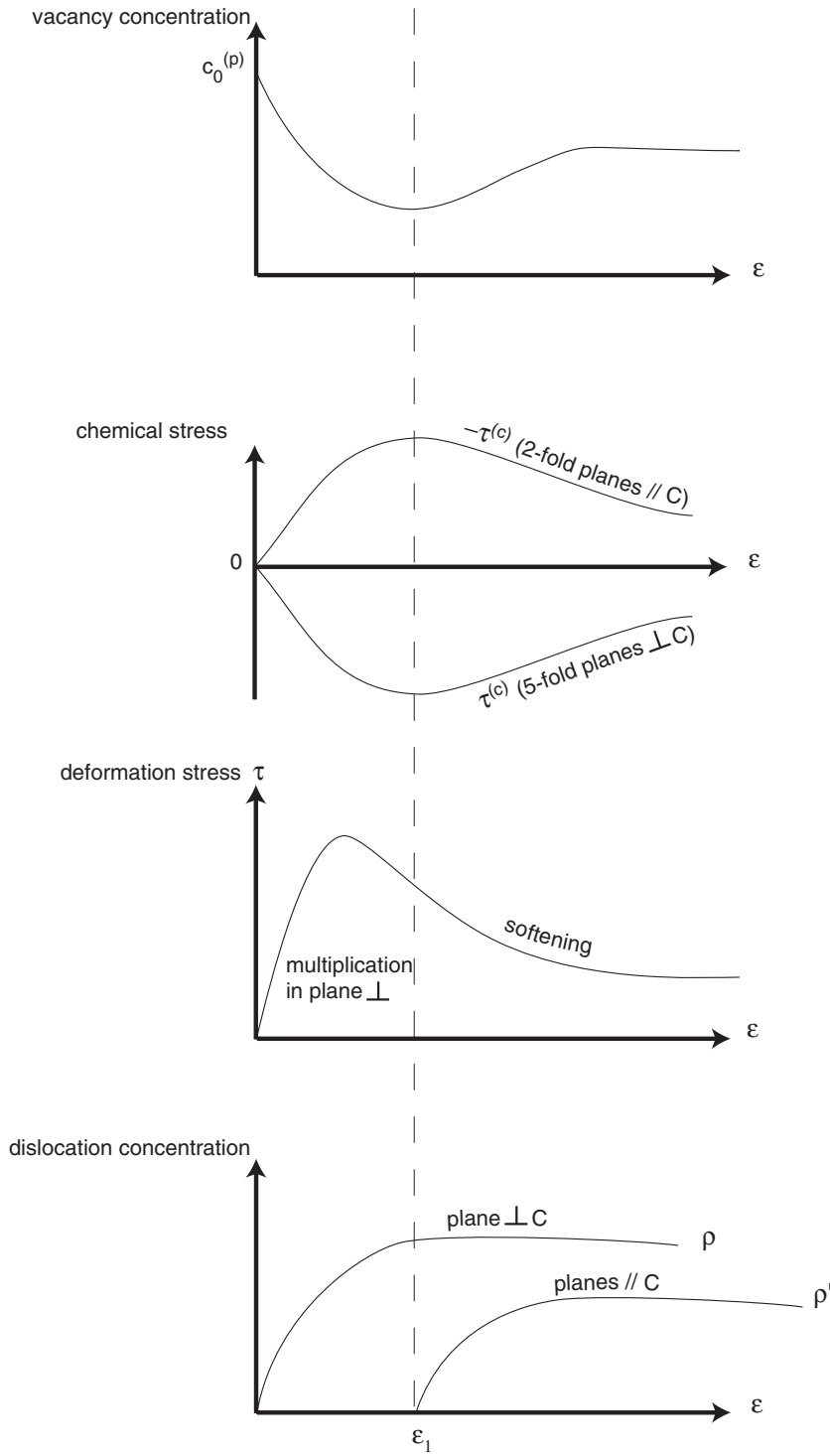

Figure 15. Schematic representations of the strain dependences of (*a*) the vacancy concentration, (*b*) the chemical stresses, (*c*) the flow stress and (*d*) the densities of dislocations in planes perpendicular and parallel to the compression axis.

(4) Superdislocations move by pure climb in fivefold planes. The two superpartials have Burgers vectors of length 0.456 nm. They are separated by a complex fault which is the projection of an APB in the physical space. The APB energy amounts to 69 mJ m^{-2}.
(5) Dislocations move by mixed climb in the wake of superdislocations in fivefold planes. They have twofold and threefold Burgers vectors. They probably result from the decomposition of fivefold dislocations, as illustrated by the observed decomposition of a fivefold superpartial of length 0.456 nm into a twofold dislocation of length 0.296 nm and a threefold superpartial of length 0.257 nm.
(6) Climb in planes almost perpendicular to the compression axis obey the Schmid law. They move by absorption of 'vacancies' (or emission of 'interstitials'). Dislocations climbing in twofold planes parallel to the compression axis are not sensitive to the applied stress. They, however, provide 'vacancies' for (or absorb 'interstitials' from) the former dislocations.
(7) Different multiplication rates of 'vacancy-sink' and 'vacancy-source' dislocations, under various chemical forces, may account for the work softening observed in quasicrystals.

Acknowledgements

We greatly acknowledge Y. Calvayrac for the difficult growth process of Al–Pd–Mn single grains, and D. Gratias for many enlightening discussions. Access to the multianvil press of Laboratoire Magmas et Volcan in Clermont-Ferrand was made possible by financial support from Centre National de la Recherche Scientifique (Instrument National de l'Institut National des Sciences de l'Univers).

References

Boudard, M., De Boissieu, M., Janot, Ch., Heger, G., Beeli, C., Nissen, H. U., Vincent, H., Ibberson, R., Audier, M., and Dubois, J. M., 1992, *J. Phys.: condens. Mater*, **50**, 10 149.

Brunner, D., Plachke, D., and Carstanjen, H. D., 2000, *Mater. Sci. Engng*, **294–296**, 773.

Caillard, D., 2000, *Quasicrystals Current Topics*, edited by E. Belin-Ferré, C. Bergé, M. Quiquandon, and A. Sadoc (Singapore: World Scientific).

Caillard, D., Mompiou, F., Bresson, L., and Gratias, D., 2003, *Scripta mater*, **49**, 11.

Caillard, D., Morniroli, J. P., Vanderschaeve, G., Bresson, L., and Gratias, D., 2002a, *Eur. Phys. J. Appl. Phys.*, **20**, 3.

Caillard, D., Roucau, C., Bresson, L., Gratias, D., 2002b, *Acta mater*, **50**, 4499.

Caillard, D., Vanderschaeve, G., Bresson, L., and Gratias, D., 1999, *Mater Res. Soc. Symp. Proc.*, **553**, 301; 2000, *Phil. Mag.* A, **80**, 237.

Cahn, J. W., Shechtman, D., and Gratias, D., 1989, *J. Mater. Res.*, **1**, 13.

Cordier, P., and Rubie, D. C., 2001, *Mater. Sci. Engng*, **A309**, 38.

Cornier-Quiquandon, M., Quivy, Lefebvre, S., Elkaim, E., Heger, G., Katz, A., and Gratias, D., 1991, *Phys. Rev.* B, **44**, 2071.

Feuerbacher, M., Klein, H., Schall, P., Bartsch, M., Messerschmidt, U., and Urban, K., 1999, *Mater. Res. Soc. Symp. Proc.*, **553**, 307.

Feueurbacher, M., Metzmacher, C., Wollgarten, M., Baufeld, B., Bartsch, M., Messerschmidt, U., and Urban, K., 1997, *Mater. Sci. Engng*, **A233**, 103.

Gevers, R., 1972, *Méthodes et Techniques Nouvelles d'Observation en Métallurgie Physique*, edited by B. Jouffrey (Paris: Société Française de Microscopie Electronique), p. 155.

Hirth, J., and Lothe, J., 1992, *Theory of Dislocations* (Malabar, Florid: R. E. Krieger), p. 557.

Howie, A., and Whelan, M. J., 1962, *Proc. R. Soc.*, **267**, 206.

MATTERSTOCK, B., CONFORTO, E., KRUML, T., BONNEVILLE, J., and MARTIN, J. L., 1999, *Mater. Res. Soc. Symp. Proc.*, **552**, KK10-3-1.
MESSERSCHMIDT, U., and BARTSCH, M., 2003, *Scripta mater*, **49**, 33.
MESSERSCHMIDT, U., GEYER, B., BARTSCH, M., FEUERBACHER, M., and URBAN, K., 1999, *Mater. Res. Soc. Symp. Proc.*, **553**, 319.
MIKULLA, R., GUMBSCH, P., and TREBIN, H. R., 1998, *Phil. Mag. Lett.*, **78**, 369.
ROSENFELD, R., FEUERBACHER, M., BAUFELD, B., BARTSCH, M., WOLLGARTEN, M., HANKE, G., BEYSS, M., MESSERSCHMIDT, U., and URBAN, K., 1995, *Phil. Mag. Lett.*, **72**, 375.
SCHAAF, G. D., MIKULLA, R., ROTH, J., and TREBIN, H.-R., 2000, *Mater. Sci. Engng*, **A294–A296**, 799.
TAKEUCHI, S., 2003, *Scripta mater*, **49**, 19.
TAKEUCHI, S., TAMURA, R., and KABUTOYA, E., 2002, *Phil. Mag.* A, **82**, 379.
TANAKA, K., MITARAI, Y., and KOIWA, M., 1996, *Phil. Mag.* A, **73**, 1715.
VIGUIER, B., and MORTENSEN, A., 2001, *Ultramicroscopy*, **87**, 123.
WANG, R., FEUERBACHER, M., WOLLGARTEN, M., and URBAN, K., 1998, *Phil. Mag.* A, **77**, 523.
WOLLGARTEN, M., BARTSCH, M., MESSERSCHMIDT, U., FEUERBACHER, M., ROSENFELD, R., BEYSS, M., and URBAN, **K**., 1995, *Phil. Mag. Lett.*, **71**, 99.
WOLLGARTEN, M., BEYSS, M., URBAN, K., LIEBERTZ, H., and KOCSTER, U., 1993, *Phys. Rev. Lett.*, **71**, 543.
WOLLGARTEN, M., GRATIAS, D., ZHANG, Z., and URBAN, K., 1991, *Phil. Mag.* A, **64**, 819.